Brain, Behavior, and Immunity 129 (2025) 279–293

Contents lists available at ScienceDirect

Brain Behavior and Immunity

journal homepage: www.elsevier.com/locate/ybrbi

Full-length Article

HDAC inhibitors engage *MITF* and the disease-associated microglia signature to enhance amyloid β uptake

Verena Haage [a,g,1], John F. Tuddenham [a,b,1], Alex Bautista [a,1], Frankie Garcia G. [a], Charles C. White [a], Ronak Patel [c,d], Natacha Comandante-Lou [a], Victoria Marshe [a], Jennifer Griffin [e], Ye Zhou [e], Deniz Ghaffari [e], Beatrice Acheson [e], Mariko Taga [a], Peter H. St George-Hyslop [d,e], Rajesh Kumar Soni [f], Peter A. Sims [b], Vilas Menon [a], Andrew A. Sproul [c], Philip L. De Jager [a,*]

[a] *Center for Translational & Computational Neuroimmunology, Department of Neurology and the Taub Institute for Research on Alzheimer's Disease and the Aging Brain, Columbia University Irving Medical Center, USA*
[b] *Department of Systems Biology, Columbia University Irving Medical Center, New York, NY, USA*
[c] *Department of Pathology and Cell Biology and the Taub Institute for Research on Alzheimer's Disease and the Aging Brain, Columbia University Irving Medical Center, USA*
[d] *Dept of Neurology, Carol and Gene Ludwig Center for Research on Neurodegeneration, and Taub at Columbia, USA*
[e] *Department of Neurology, University Health Network and Temerty Faculty of Medicine, Tanz, University Of Toronto, Toronto, Ontario, Canada*
[f] *Proteomics and Macromolecular Crystallography Shared Resource, Herbert Irving Comprehensive Cancer Center, New York, NY, USA*
[g] *Experimental and Clinical Research Center, Max Delbrueck Center for Molecular Medicine and Charité-Universitätsmedizin Berlin, Berlin, Germany*

ARTICLE INFO

Keywords:
Disease-associated microglia (DAM)
In vitro model systems
Human microglia
Pharmacological modelling
Functional analysis

ABSTRACT

Disease-associated microglia (DAM), initially described in mouse models of neurodegenerative diseases, have been classified into two related states; starting from a TREM2-independent DAM1 state to a TREM2dependent state termed DAM2, with each state being characterized by the expression of specific marker genes (Keren-Shaul, 2017). Recently, single-cell (sc)RNA-Seq studies have reported the existence of DAM in humans (Pettas, 2022; Jauregui, 2023; Friedman, 2018; Mathys, 2019; Tuddenham, 2024); however, whether DAM play beneficial or detrimental roles in the context of neurodegeneration is still under debate (Butovsky and Weiner, 2018; Wang and Colonna, 2019). Here, we present a pharmacological approach to mimic human DAM *in vitro*: we validated *in silico* predictions that two different histone deacetylase (HDAC) inhibitors, Entinostat and Vorinostat, recapitulate aspects of the DAM signature in two human microglia-like model systems. HDAC inhibition increases RNA expression of *MITF*, a transcription factor previously described as a regulator of the DAM signature (Dolan, 2023). This engagement of *MITF* appears to be associated with one part of the DAM signature, refining our understanding of the DAM signature as a combination of at least two transcriptional programs that appear to be correlated *in vivo*. Further, we functionally characterized our DAM-like model system, showing that the upregulation of this transcriptional program by HDAC inhibitors leads to an upregulation of amyloid β and pHrodo Dextran uptake – while E.coli uptake is reduced – and a specific reduction of MCP1 secretion in response to IFN-γ and TNF-α. Enhanced amyloid β uptake was confirmed in iPSC-derived microglia. Overall, our strategy for compound-driven microglial polarization offers potential for exploring the function of human DAM and for an immunomodulatory strategy around HDAC inhibition.

1. Introduction

Disease-associated microglia (DAM) were first described in mouse models of neurodegenerative diseases and were proposed to exist in two related states: there is an initial DAM1 state that transitions to a TREM2-dependent state termed DAM2. The DAM1 and DAM2 states are

* Corresponding author.
E-mail address: pld2115@cumc.columbia.edu (P.L. De Jager).
[1] Denotes equal contributions.

https://doi.org/10.1016/j.bbi.2025.05.027
Received 15 January 2025; Received in revised form 14 May 2025; Accepted 27 May 2025
Available online 30 May 2025

characterized by the expression of specific marker genes (Keren-Shaul et al., 2017). Only recently, single-cell (sc)RNA-Seq studies have reported the existence of DAM in humans (Pettas et al., 2022; Jauregui et al., 2023; Friedman et al., 2018; Mathys et al., 2019; Tuddenham et al., 2024). Nevertheless, the question of whether DAM play a beneficial or detrimental role in the context of neurodegeneration remains a subject of debate (Butovsky and Weiner, 2018; Wang and Colonna, 2019). To date, only one study has proposed an *in vitro* model system for human DAM based on the exposure of induced pluripotent stem cell-derived microglia-like cells (iMGs) to apoptotic neurons, and the investigators used this model system to assess the phagocytic capacity of these perturbed cells and to propose the transcription factor MITF as a regulator of the DAM signature (Dolan et al., 2023). This model system is a very interesting foray into modeling human DAM but is limited by the nature of the polarizing agent since it is derived from biological material and therefore varies over production batches and tissue sources.

Here, we present an alternative, pharmacological approach to mimic human DAM *in vitro*, prioritizing tool compounds using an *in silico* screening methodology. We first show that DAM1-like and DAM2-like signatures exist in single-cell and single-nucleus RNA sequencing datasets derived from human microglia and then that we can prioritize and validate compounds which reproduce DAM-like transcriptional signatures in human microglia-like cells *in vitro*. Namely, we report that two different histone deacetylase (HDAC) inhibitors lead to higher *MITF* expression, engagement of DAM-like signatures, and functional changes in the target cells (altered phagocytosis and response to inflammatory stimuli). Further, we begin to dissect the human DAM signature into its component parts: it appears to consist of at least two transcriptional programs. We therefore extend a growing pharmacological toolkit for the microglia community (Tuddenham et al., 2024; Haage et al., 2024) and illustrate our model system's potential to further explore human DAM biology.

2. Results

2.1. Definition of DAM signatures analyzed in this study

We recently generated two datasets derived from single-cell RNA sequencing (scRNAseq) of freshly isolated live primary human microglia derived from 74 donors (Tuddenham et al., 2024) and single-nucleus RNA sequencing (snRNAseq) profiling of frozen dorsolateral prefrontal cortex from 437 aging and Alzheimer brains (Green et al., 2024). Both of these independent datasets identified a human microglial subtype that is enriched for the DAM2 signature: cluster 11 among the live microglia profiled with scRNAseq (Tuddenham et al., 2024) (Fig. 1**A**) and microglia 13 in the snRNAseq data (Green et al., 2024) (Fig. 1**B**).

Here, using the selection of genes prioritized in the original mouse DAM publication (Keren-Shaul et al., 2017), we further evaluate DAM-enriched human microglial subtypes by assessing the expression of these selected DAM1 (*APOE, H2-D1, B2M, FTH1, CSTB, LYZ2, CTSB, TYROBP, TIMP2, CTSD*) and DAM2 (*ANK, CD9, CD63, SERPINE2, SPP1, CADM1, CD68, CTSZ, AXL, CLEC7A, CTSA, CD52, CSF1, CCL6, LPL, CTSL, CST7, ITGAX, GUSB, HIF1A*) signature genes (Keren-Shaul et al., 2017) from mouse across our single-cell and single-nucleus human microglial datasets (Tuddenham et al., 2024; Green et al., 2024) (Fig. 1**C-D**). Following gene set enrichment analysis for each set of signature genes (DAM1, DAM2), the log-normalized expression of each set was plotted into the respective UMAP of the human microglial sc- or snRNAseq data. Interestingly, we detected both DAM1 and DAM2 marker gene expression. While the DAM1 signature was more broadly expressed among human microglia, DAM2 expression was restricted to more defined groups of cells, characterized by increased expression of *LPL, LGALS1, CD9* and *GPNMB* (Fig. 1**C-D, Fig. S1**). These DAM2+ cells include cluster 11 in live microglia, identified as the DAM-enriched cluster in the earlier report (Tuddenham et al., 2024).

With regards to the snRNAseq dataset, DAM1 gene expression was more restricted to certain aspects of the distribution of microglia, as was DAM2 (Fig. 1**C-D**). Interestingly, as also observed in the scRNAseq data, microglia with DAM2-specific expression were enriched in a region of the distribution of microglia that is high in DAM1 marker expression, suggesting that DAM2 might arise from DAM1, but that not all microglia transition from a DAM1 to a DAM2 state. At this point, the role of the observed DAM-like signatures needs to be validated. In this large snRNASeq dataset, both the DAM1-enriched and the DAM2-enriched microglia are associated with the amyloid and tau proteinopathies that define AD (Green et al., 2024).

2.2. Identifying compounds that recapitulate the DAM signatures

To establish a model system using human cells, we deployed an *in silico* compound prioritization strategy to identify pharmacological compounds that may either induce or suppress the respective DAM-like signatures identified in the human datasets, with the goal of recapitulating and manipulating those cell subsets *in vitro* and to evaluate their function as we have previously done for other microglial subtypes (Haage et al., 2024). In short, we leveraged the Connectivity Map resource (CMAP) (Subramanian et al., 2017), a transcriptomic atlas derived from a range of human cell lines exposed to thousands of pharmacological compounds, to identify molecules that induce or reduce the transcriptomic signature of our DAM-like human microglial subtypes identified from the sc- (cluster 11 (Tuddenham et al., 2024), for full signature see **Table S1**) or the snRNAseq datasets (microglia 13^{11}, Fig. 2**A,** for full signature see **Table S1**). Our analysis yielded a specific set of compounds for each of the queried DAM signatures (excerpt of selected compounds in Fig. 2**B,** for full list see **Fig. S2A and Table S2A-B**). To select candidate compounds, the common upregulated or downregulated genes from the two analyses were prioritized, and we selected five to six predicted compounds from each comparison based on an absolute tau score > 99.5. The focus of this analysis was initially to identify compounds mimicking a more general DAM-like human signature instead of building specific DAM1 and DAM2 *in vitro* models since we did not want to overfit our modeling to the primarily mouse-defined signatures (Keren-Shaul et al., 2017).

Our analysis identified a series of intriguing compounds (Fig. 2**B**). One of the top families of positive regulators in our screen were histone deacetylase (HDAC) inhibitors, including Entinostat and the FDA-approved Vorinostat, as well as experimental compounds such as Merck60 and APHA-compound-8. Interestingly, except for Vorinostat, which is a pan-HDAC inhibitor, many of these drugs are selective HDAC inhibitors, with HDAC 1/2 being the most common targets (Eckschlager et al., 2017). Additional compounds predicted to induce the DAM-like signature include the neural Wiskott-Aldrich syndrome protein (N-WASP) inhibitor Wiskostatin, the tricyclic antidepressant Trimipramine and the hypoxia-inducible factor (HIF) inhibitor Flavokavain B (Fig. 2**B**). It is interesting to note that HIF-1α was previously predicted as an upstream regulator of amyloid plaque-associated microglia and has been shown to regulate synaptosomal phagocytosis *in vitro* (Grubman et al., 2021).

As compounds that downregulate the DAM signature, our *in silico* analysis identified: Geranylgeraniol (an intermediate in the mevalonate pathway), valproic acid (an established treatment for seizures), cholic acid (a naturally occurring bile acid), Ramipril (an angiotensin-converting enzyme (ACE) inhibitor), the prodrug Temozolomide (an alkylating agent currently used in glioblastoma therapy (Stupp et al., 2005) and Naftopidil (an α1-Adrenoceptor Antagonist) (Fig. 2**B**).

2.3. Validation of prioritized compounds in the human HMC3 model system

In order to assess the effect of the selected compounds on the expression of DAM signature genes, the compounds were first titrated on the human microglia cell 3 (HMC3) microglia-like cell line to determine

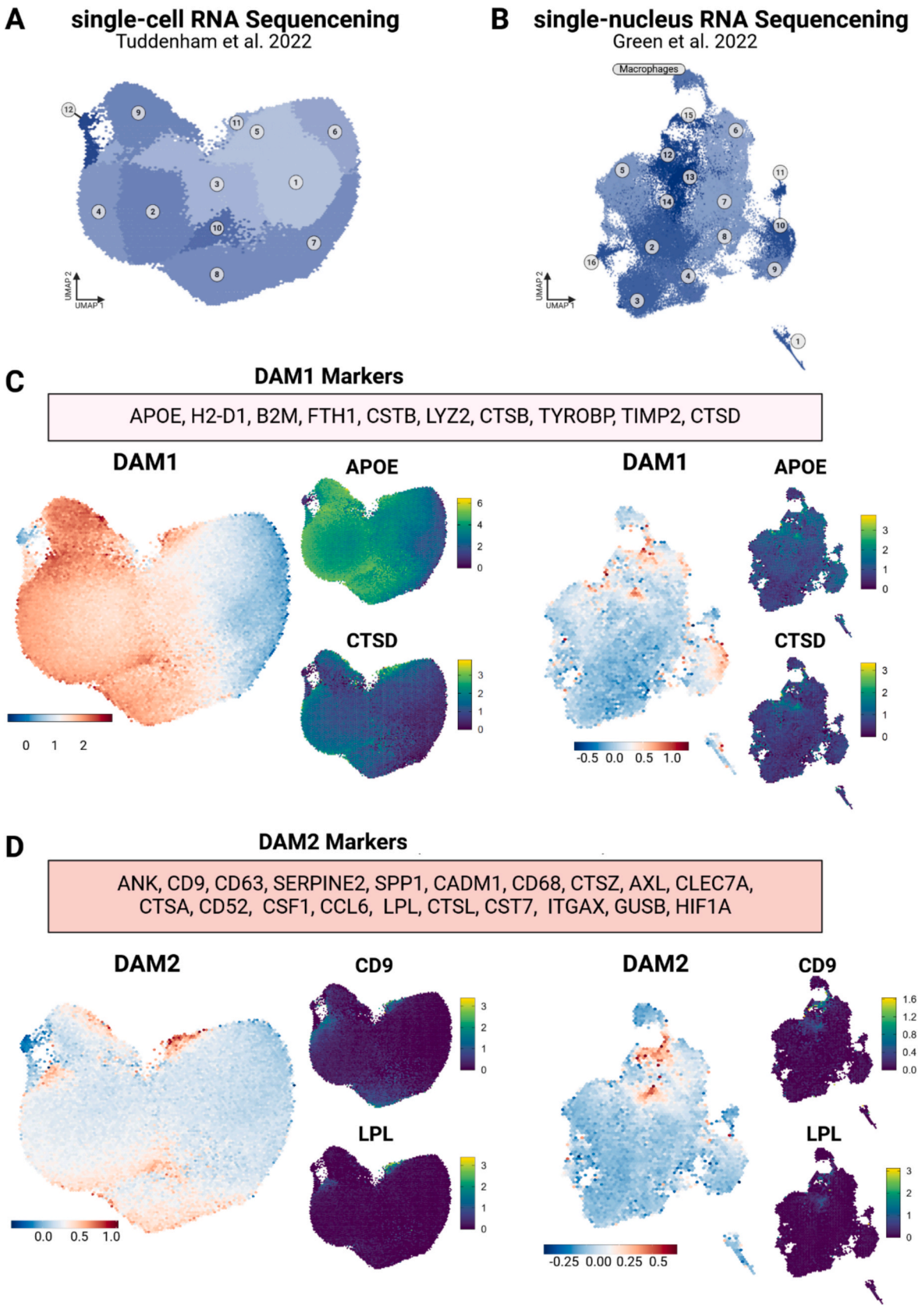

(caption on next page)

Fig. 1. Examining the disease-associated microglial (DAM) signature across human microglia identifies different patterns of capture of DAM-associated genes between single-cell (sc-) (Tuddenham et al., 2024) and single-nucleus (sn-) RNAseq (Green et al., 2024) data. **A. UMAP of human single-cell microglial clusters** (Tuddenham et al., 2024)**.** Here, microglia from a single-cell dataset derived from 74 human donors are plotted. 12 microglial clusters were identified. **B. UMAP of human single-nucleus microglial clusters** (Green et al., 2024)**.** Here, microglia from a single-nucleus dataset derived from 437 human donors are plotted. 16 microglial clusters were identified. **C. DAM1 module expression across the sc- (left) and sn- (right) RNAseq datasets.** Enrichment of the top 10 genes for the DAM1 signature or the top 20 genes for the DAM2 signature from the original publication was calculated on a per-cell basis. Module scores were computed compared to background genes with similar levels of expression. Individual cells are colored by log-fold change of the gene set. Module scores were plotted on hex-binned UMAPs. Individual hexagons are aggregates of 50 cells on average, the plotted score per hexagon is the mean of the score across all cells aggregated within each hexagon. Scores are log-normalized counts, as shown on the color gradient bar. Red/yellow represents the maximal expressed value, while blue/purple represents the lowest expression values. Selected DAM1 (*APOE*, *CTSD*) marker genes were plotted across microglial clusters. **D. DAM2 module expression across the sc- (left)** (Tuddenham et al., 2024) **and sn- (right)** (Green et al., 2024) **RNAseq datasets.** Enrichment of the top 10 genes for the DAM1 signature or the top 20 genes for the DAM2 signature from the original publication was calculated on a per-cell basis. Module scores were computed compared to background genes with similar levels of expression. Individual cells are colored by log-fold change of the gene set. Module scores were plotted on hex-binned UMAPs. Individual hexagons are aggregates of 50 cells on average, the plotted score per hexagon is the mean of the score across all cells aggregated within each hexagon. Scores are log-normalized counts, as shown on the color gradient bar. Red/yellow represents the maximal expressed value, while blue/purple represents the lowest expression values. Selected DAM2 (*CD9, LPL*) marker genes were plotted across microglial clusters. (For interpretation of the references to color in this figure legend, the reader is referred to the web version of this article.)

doses for each of the compounds that were not toxic to the cells. Specifically, an MTT (3-[4,5-dimethylthiazol-2-yl]-2,5 diphenyl tetrazolium bromide) assay was used and drug concentrations with a comparable absorption to DMSO-treated HMC3 microglia (control condition) were selected for downstream experiments (**Fig. S2B-C**). Following the selection of the treatment concentration for each drug, HMC3 microglia were exposed for 6hrs and 24hrs. Subsequently, the expression of *CTSD* (DAM1 marker) as well as *SPP1* and *CD9* (DAM2 marker genes) were assessed via RT-qPCR (Fig. 2**C**). With regards to the compounds predicted to induce the DAM signature, we identified the two HDAC-inhibitors Vorinostat and Entinostat as our top candidates. We detected significant upregulation of *SPP1* expression, particularly after 24 h, with Vorinostat ($p = 0.0009$) and Entinostat ($p < 0.0001$). The effect on *CD9* was more modest: at 6 h for Vorinostat ($p = 0.014$) and at 24 h for Entinostat ($p = 0.038$). As both compounds belonged to the class of HDAC inhibitors and showed significant effects with our screening markers, Vorinostat and Entinostat were selected for further validation experiments. HDAC inhibitors have primarily been studied in cancer; however, there is growing interest in their use in the field of neurodegeneration (Shukla and Tekwani, 2020). They have previously been shown to suppress inflammatory responses in microglia (Kannan et al., 2013).

As it is currently unclear whether DAMs play a beneficial or detrimental role in humans, the identification of compounds with the potential to downregulate the DAM-like signature is also of great interest. However, from our selected candidate compounds none showed a consistent pattern of downregulating the expression of DAM signature genes (Fig. 2**C**, lower panel). We therefore proceeded with the DAM-inducing drugs focusing on the development of a human DAM *in vitro* model system and the functional characterization of DAM-like cells.

In order to further assess the effect of Vorinostat and Entinostat treatment on the HMC3 microglial-like cell line, we exposed three independent passages of HMC3 microglia to each of the drugs for 24 h and generated bulk RNA-Seq data for each compound. Following Principal Component analysis (PCA), Entinostat-treated cell samples clustered closely together and were distinct from DMSO-treated cells, while Vorinostat-treated samples clustered between the other two conditions (Fig. 3**C**). For analysis, we used the DESeq2 (Love et al., 2014) package implemented within R (4.4.1) to test for differentially expressed genes between the DMSO-treated and compound-treated conditions. Subsequently, we assessed the expression of different DAM or DAM-like gene sets, namely the mouse-derived DAM1 and DAM2 (Keren-Shaul et al., 2017), as well as gene sets defining microglial cluster 11 (from scRNAseq data) (Tuddenham et al., 2024) and the microglia 13^{11} subtype (from snucRNAseq data) that were empirically defined from recent human datasets (**Table S3A**). To do so, a Wald test was performed and we implemented a Benjamini-Hochberg (FDR) value to correct for the testing of multiple hypotheses; each gene set was analyzed independently from the others (Fig. 3). After applying this test, any gene with a positive log2 fold-change (FC) and an FDR <0.05 was considered to be statistically significantly upregulated. For a comparison between the different queried signatures, see **Fig. S3A**. For a full list of differentially expressed genes between the different treatment conditions, see **Table S4A-E**.

When assessing the microglial cluster 11 signature (Tuddenham et al., 2024), we noticed that a portion of these markers was highly expressed at baseline by DMSO control cells (Fig. 3**A**). While Vorinostat significantly induced the expression of 26/89 (29 %) cluster 11 marker genes, Entinostat exposure engaged a broader set of genes, significantly inducing 37/89 (42 %) markers that are not expressed under the control condition (DMSO). These data clearly suggest that the DAM signatures are composed of at least two sets of genes whose transcriptional regulation is somewhat distinct: these two sets of genes may be co-regulated in the *ex vivo* contexts from which they were derived, but our molecularly precise perturbation reveals a difference in regulation of these genes. Thus, the cluster 11 signature likely contains several distinct transcriptional programs that share regulatory signals in certain contexts, one of which seems to be engaged at baseline by the HMC3 culture system. Overall, *CD9*, *PADI2*, *GSN* and *CTSB* (Fig. 3**B**) among others were genes strongly induced by both compounds. *CD9* is a key DAM marker gene (Keren-Shaul et al., 2017), while *PADI2* has been associated with neurodegeneration in microglia (Asaga and Ishigami, 2007). *CTSB* has been reported as a potential major driver of brain aging (Nakanishi, 2020).

When assessing the expression of the microglia 13 signature (Green et al., 2024), we also observed a minor subset of these signature genes being expressed under baseline conditions (DMSO control), and they were downregulated upon Entinostat treatment and slightly reduced upon Vorinostat exposure (Fig. 3**A**. However, the majority of the microglia 13 gene signature is engaged by our HDAC inhibitors: Entinostat potently and significantly induced 65/127 of Microglia 13 genes, which is 51 % of the signature. Similar to the results from cluster 11, Vorinostat significantly induced a lower percentage of genes belonging to the microglia 13 signature (23/127 genes; 18 % of the signature). Notably, both Vorinostat and Entinostat induced *PADI2*: Vorinostat, $p_{adjusted} = 3.69E^{-36}$, and Entinostat, $p_{adjusted} = 2.97E^{-78}$. Most significantly, they also both induced *MITF (*Vorinostat – padj $= 9.01E^{-28}$; Entinostat – padj $= 1.19E^{-23}$*)*, a transcription factor recently shown to be an important driver of the DAM signature and a highly phagocytic phenotype in human iPSC-derived microglia-like cells (Dolan et al., 2023) (Fig. 3**B**).

When assessing the expression of the original mouse DAM1 and DAM2 signatures (Keren-Shaul et al., 2017), we also observed that a small fraction of those genes are expressed by DMSO-treated control cells (Fig. 3**A)**. We further observed a significant induction of both signatures by Entinostat: about 63 % of each signature is engaged (DAM1:

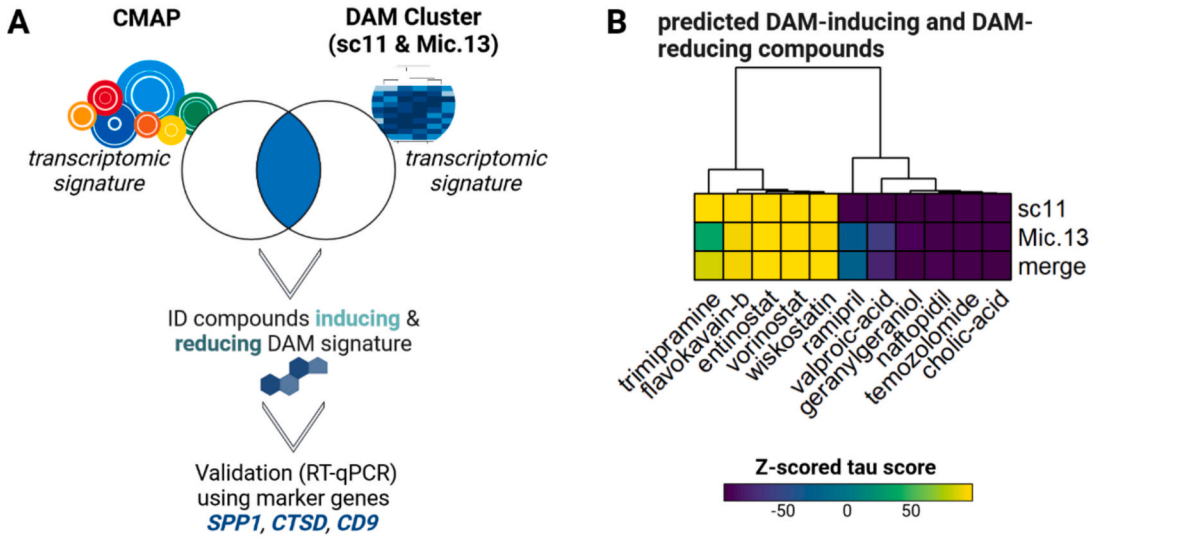

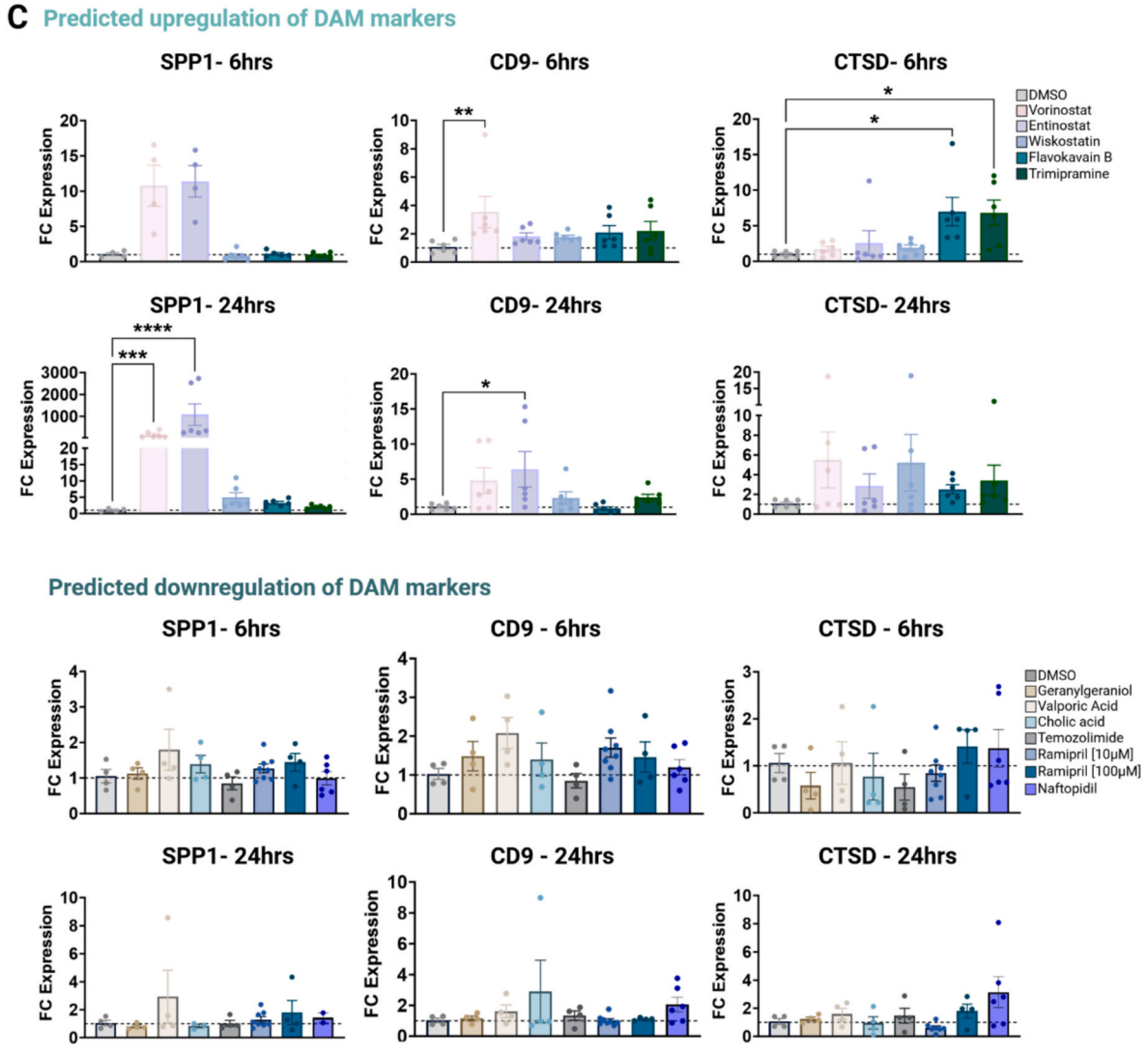

(caption on next page)

Fig. 2. *In silico* compound screen and validation of transcriptomic modulators for the DAM1/DAM2 signature. **A. Graph depicting the *in silico* approach** to identify compounds mimicking the DAM cluster signatures using the CMAP resource (Connectivity Map resource; [13]) followed by a validation approach. **B. CMAP predictions** from microglial single-cell RNA-Seq Cluster 11 (Tuddenham et al., 2024), single-nucleus RNA-Seq Microglia 13 cluster (Green et al., 2024), and the overlapping upregulated gene set. The Connectivity Map (CMAP) was used to identify compounds that are predicted to upregulate or downregulate gene sets associated with either of the DAM-like clusters from single-cell or single-nucleus data. Heatmaps depict the Z-scored tau score for each compound following query analysis. Clustering of tau scores across microglial clusters 11, 13, or the merged signature was performed with absolute linkage. **C. Screening of identified candidate drugs via RT-qPCR in HMC3 microglia-like cells.** HMC3 cells were exposed to selected compounds predicted to upregulate (upper panel; DMSO control (1:1000–1:10.000): n = 6; Vorinostat (1 μM): n = 6; Entinostat (10 μM): n = 6; Wiskostatin (1 μM): n = 6; Flavokavain B (10 μM): n = 6; Trimipramine (10 μM): n = 6;) or downregulate (lower panel; DMSO control (1:1000–1:10.000): n = 4; Geranylgeraniol (10 μM): n = 4; Valproic acid (0.9 μg/ml): n = 4; Cholic acid (10 μM): n = 4; Temozolomide (100 μM): n = 4; Ramipril (10 μM): 0.01 mM n = 8, 0.1 mM n = 4; Naftopidil (10 μM): n = 6) the DAM signature at 6 hrs. or 24 hrs. Selected DAM marker gene expression (*CD9, SPP1, CTSD*) was assessed via RT-qPCR. CT values were normalized to *HPRT1*. Bars represent fold-change gene expression in relation to DMSO control. For statistical analysis Kruskal Wallis test followed by Dunn's multiple comparisons test was performed.*p.adj ≤ 0.05; **p.adj ≤ 0.01; ***p.adj ≤ 0.001; ****p.adj ≤ 0.0001. (For interpretation of the references to color in this figure legend, the reader is referred to the web version of this article.)

5/8 genes; DAM2:10/16 genes). On the other hand, Vorinostat significantly induced 63 % of the DAM1 and 38 % of the DAM2 signatures (DAM1: 5/8 genes; DAM2: 6/16 genes). Both compounds induced *APOE*, *B2M*, *TIMP2, CTSB, FTH1* as DAM1 markers as well as the DAM2 markers *SPP1*, *LPL*, *ITGAX*, *CD9*, *CD52* and *CADM1* (Fig. 3**E;** Table 1). Fig. 3**D** depicts an overview of the percentage of markers from each signature that are significantly induced by each compound (Vorinostat, Entinostat). Fig. 3**E** provides an overview of signature-specific markers induced by both compounds: Vorinostat and Entinostat. Table 1 provides a detailed overview of all the genes induced by one or both HDAC inhibitors, grouped into the assessed signatures.

Overall, our two prioritized HDAC inhibitors engage overlapping aspects of the DAM-like signatures; however, these signatures appear to be complex, consisting of at least 2 sets of genes representing distinct transcriptional programs, one of which is upregulated in the DMSO control condition. The second, larger gene set includes the key marker genes for DAMs and is engaged by these compounds. This is not surprising as microglia and microglia-like cells are highly reactive and are unlikely to be in a homeostatic state in culture (Cadiz et al., 2022). Nonetheless, the HDAC inhibitors clearly engage an important component of the DAM-like signatures, and these signatures need to be refined to guide future study designs.

2.4. Evaluation of Vorinostat in the iMG model system

To assess the robustness of the effect of our putative tool compounds, we tested one of the DAM-inducing compounds, Vorinostat, using the induced pluripotent stem cell (iPSC)-derived microglia-like system (iMG) on Day 28–29 of the iMG differentiation protocol (Abud et al., 2017; McQuade et al., 2018) (detailed description in **Methods**). Following 24 h of exposure to Vorinostat, iMG from two independent differentiations were harvested and subjected to bulk RNA sequence profiling followed by an analysis assessing the expression of four different marker sets (Fig. 4) using the same approach as previously described for HMC3 microglia (Fig. 3). In addition to the DAM1/DAM2, cluster 11 and microglia 13 signatures tested above (Keren-Shaul et al., 2017; Tuddenham et al., 2024; Green et al., 2024), we also assessed the expression of signature genes recently derived from an iMG-derived human DAM model following exposure to a preparation of apoptotic neurons among other tested brain intrinsic substrates (Dolan et al., 2023) (**Fig. S4A; Table S3B**). The authors of that report identified two cell clusters related to the DAM subtype, which they termed Cluster 2 and 8. As a result, we refer to this signature as iMG Cluster $2 + 8$[9] for the purpose of this manuscript. Fig. 4**A** depicts an overview of upregulated genes for the most relevant signatures assessed in the iMG model system (cluster11 (Tuddenham et al., 2024), microglia 13[11], iMG $2 + 8$[9]), while Fig. 4**B** depicts the corresponding heatmaps for the signatures that we evaluated.

While Vorinostat treatment of iMGs induced some marker genes from each of the signatures which we did not previously detect in Vorinostat- or Entinostat-treated HMC3 microglia-like cells (cluster 11: *DHRS9*, *GYPC, OLR1, RABAC, SCARB2;* microglia 13*: AOAH, OLR1, PTPRG;* DAM1/2*: CSF1, CTSA*), we focused our subsequent analysis on the genes that emerged from the previous HMC3 experiments as upregulated following Vorinostat- or Entinostat-treatment (depicted in Table 1) so as to validate our findings in a second model system. Table 2 presents a subset of genes from Table 1 which we could validate in the Vorinostat-treated iMG model system. We confirmed an upregulation of 4 Cluster 11 signature genes, 12 Microglia 13 genes, three DAM1/2 gene and 16 iMG2 + 8 genes, including the previously published DAM-relevant transcription factor *MITF* (Dolan et al., 2023). Fig. 4**C** highlights the significantly upregulated genes for each of the queried signatures in Vorinostat-treated iMGs, thereby providing an overview of the validated subset of DAM-like genes across our two model systems. In addition to *MITF*, we identified *LIPA*, *NPL* and *CADM1* as the most consistent DAM-like markers upregulated across our model systems.

A full list of differentially expressed genes across different treatment conditions and model systems is provided under **Table S4A-E**.

2.5. MITF expression in the DAM model systems

The most interesting result is *MITF*, given that it has been proposed to be a regulator of the DAM signature by other investigators (Dolan et al., 2023) and is a member of the microglial 13 signature (Supplementary Table 1) (Green et al., 2024). Vorinostat and Entinostat induced a highly significant increase in *MITF* expression in HMC3 microglia (One-way ANOVA followed by Dunnett's multiple comparisons test; Vorinostat: p = 0.0008; Entinostat: p = 0.0008)(Fig. 4**D**). The Vorinostat-induced increase in *MITF* expression was also observed in our iMG-DAM model (Unpaired *t*-test, Vorinostat – p = 0.0406). Thus, the effect appears to be preserved across the two DAM model systems. These data strengthen the validity of our model system with regards to prior reports of the role of *MITF* in driving a disease-associated microglia like signature and a highly phagocytic phenotype (Dolan et al., 2023). We therefore turned to the functional evaluation of our compound-driven DAM-like cells, one of the primary goals of establishing an *in vitro* model for human DAM.

2.6. Functional characterization of the HDAC-inhibitor induced in vitro DAM model

To assess the phagocytic phenotypes of our HMC3 microglia-like cells, we pretreated cells with Vorinostat, Entinostat or DMSO (control) for 24 h. This was followed by exposure to three distinct substrates: pHrodo Dextran to monitor macropinocytosis, fluorescently labeled Amyloid beta (Aβ) to assess a phagocytic phenotype relevant to amyloid proteinopathy as well as pHrodo-labeled Escherichia coli (E. coli) to assess a phagocytic response associated with acute neuroinflammation. Flow-cytometry was used as a readout (Fig. 5**A; Fig. S5A**). As an additional control, we pretreated the cells with Cytochalasin D (**Fig. S5B**). When assessing macropinocytosis through pHrodo Dextran uptake, we observed a significant upregulation of uptake in both Vorinostat- and Entinostat-treated HMC3 cells, with Vorinostat showing a slightly higher increase (Fig. 5**B**). When assessing the uptake of Aβ, both compounds also showed an increase in Aβ uptake in comparison to DMSO control,

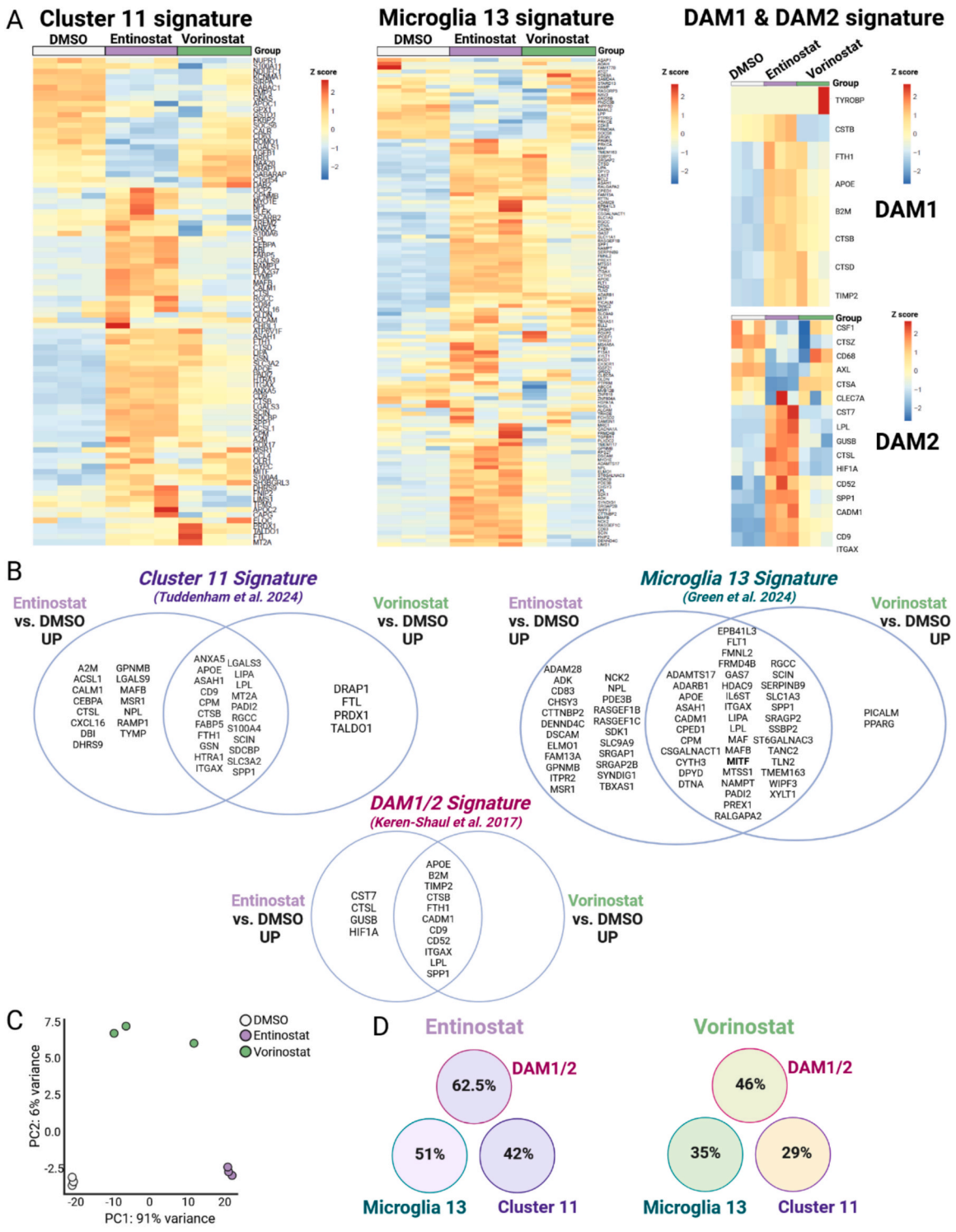

(caption on next page)

Fig. 3. Bulk RNAseq data from the HMC3 DAM model. **A. Heatmaps showing the expression of Cluster 11[6]** (left), **Microglia 13[11]** (middle) and **DAM1/DAM2** (Keren-Shaul et al., 2017) (right) **marker gene sets** in bulk RNAseq data generated 24hrs following exposure to DMSO (control; 1:1000 for Entinostat; 1:10.000 for Vorinostat), Entinostat (purple; 10 μM) or Vorinostat (green; 1 μM). Each column represents a single sample, each row a single gene represented in the respective marker set. Pairwise differential testing between DMSO control and each of the treatment conditions (Entinostat, 10 μM; Vorinostat, 1 μM) was conducted using a Wald test with the Benjamini-Hochberg correction (FDR alpha < 0.05). The legend represents Z scores, with lower scores indicated in red and higher scores indicated in blue. Data represents n = 3 independent experiments for each treatment group with each n for all compounds being performed at the same time. **B. Venn diagrams depicting significantly upregulated genes across different signatures (DAM1/DAM2[1], Cluster 11[6], Microglia 13[11]) comparing significantly induced signature genes by each treatment condition (Entinostat or Vorinostat)** relative **to its DMSO control.** HMC3 microglia were treated for 24hrs with DMSO as control (1:1000 for Entinostat; 1:10.000 for Vorinostat), Entinostat (10 μM) or Vorinostat (1 μM) followed by bulk RNA-Seq. Venn diagrams were constructed based on log2 fold change (FC) expression and padj. **C. PCA plot of bulk RNAseq results from HMC3 microglia treated with DMSO, Vorinostat or Entinostat**. Principal component analysis (PCA) was calculated on log-normalized bulk RNA-Seq data derived from compound-treated HMC3 microglia following 24hrs of exposure to DMSO (control; 1:1000 for Entinostat; 1:10.000 for Vorinostat; white), Entinostat (10 μM; purple) or Vorinostat (1 μM; green). Data represents n = 3 independent experiments for each of the treatment group with each n for all compounds being performed at the same time. **D. Venn diagrams depicting the number of significantly upregulated genes by Entinostat or Vorinostat for each of the queried marker signatures DAM1 and DAM2[1], Cluster 11[6], Microglia 13[11].** The number of significantly upregulated genes across all three replicates for each treatment group (Entinostat or Vorinostat) in comparison to DMSO control was identified and converted to a percentage of marker genes upregulated/ marker set. Data for DAM1 and DAM2 depicted in purple, for Cluster 11 depicted in violet and for Microglia 13 depicted in teal. **E. Signature-specific markers induced by Vorinostat and Entinostat.** Markers significantly induced by Vorinostat and Entinostat for each signatured are depicted for DAM1/2 (purple/red) (Keren-Shaul et al., 2017), Cluster 11 (violet) (Tuddenham et al., 2024), Microglia 13 (teal) (Green et al., 2024). (For interpretation of the references to color in this figure legend, the reader is referred to the web version of this article.)

with Vorinostat ($p \leq 0.0001$) inducing again a more pronounced effect than Entinostat ($p = 0.0274$)(Fig. 5**C**). Interestingly, Aβ can be taken up via macropinocytosis and phagocytosis (Maguire et al., 2022). Thus, our two HDAC inhibitors revealed a specialization towards an increased uptake of soluble substrates, as E. coli phagocytosis was significantly decreased in Vorinostat-treated cells. Entinostat-treated cells did not show a significant decrease in E. coli uptake, although there was a trend in that direction (Fig. 5**C**). These effects on Aβ uptake are consistent with the prior report of *MITF* expression contributing to greater phagocytosis (Dolan et al., 2023).

To validate the functional consequences of HDAC inhibitor treatment in a different microglia-like model system, we assessed the uptake of Aß in iPSC-derived human microglia (iMGs; **Fig. S6**). Specifically, we elected to expose iMGs for 24 h to different concentrations of Vorinostat (0.05 μM, 1 μM and 0.5 μM) and to subsequently assess their phagocytic capacity using pHrodoRED-conjugated (RFP-) Aß 1–42 fibrils and the BioTek Cytation 5 platform (**Fig. S6**). Three independent experiments were conducted; we started by testing two doses of Vorinostat (0.1 and 0.5 μM). As we suspected some toxicity of the higher dose, we added an additional lower dose (0.05 μM) to the second and third experiments.

For the primary analysis, we used Dunnett's test to compare the proportion of cells that exceeded the median value of the mean fluorescence intensity (MFI) in the DMSO condition at the end of the experiment. We then combined the results of the individual experiments for each dose using a Fishers *meta*-analysis approach (Supplementary Table S5**, Fig. S7A-C**), and we see that both, the 0.05 μM ($p = 1.94 \times 10^{-7}$) and 0.1 μM ($p = 1.07 \times 10^{-9}$) Vorinostat doses yield a significant increase in the uptake of Aß1-42 fibrils, confirming the functional changes seen in HMC3 results (Fig. S7).

One of the limitations of the iMG model system is its variability (Hasselmann and Blurton-Jones, 2020; Stöberl et al., 2023), and we have seen this in our experiments, particularly at the two higher doses of Vorinostat. We therefore also ran a secondary analysis using a statistically more conservative random effects analysis model that accounts for inter-experimental heterogeneity. In this secondary analysis, the 0.5 μM Vorinostat condition results remain non-significant, as expected. The 0.1 μM Vorinostat dose condition results are heterogeneous, and, while the effect direction and magnitude remain similar (beta = 0.0491) (Supplementary Table S5, Fig. S7**D-F**), the summary evidence of the three experiments is not significant ($p = 0.19$). However, the 0.05 μM Vorinostat dose results remains significant, as both the second and third experiments return very consistent results (beta = 0.0486, $p = 0.0009$). Importantly, we note that the effect size of Vorinostat is virtually identical for the 0.1 and 0.05 μM doses (beta = 0.0491 and 0.0486 respectively), further supporting the robustness of the effect of Vorinostat in enhancing Aß 1–42 phagocytosis, even when we deploy a very conservative statistical model.

To complement our evaluation of phagocytosis, we also evaluated another microglial function: amplification and orchestration of immune responses. We therefore assayed the response of our HMC3 model system to stimulation with two pro-inflammatory cytokines that play an important in brain and systemic inflammation: TNF-α and IFN-γ. Specifically, we measured a panel of 15 pro-inflammatory cytokines after 12 and 24 h of stimulation with TNF-α or IFN-γ. While the secretion of 14 of the cytokines remained unaffected (**Fig. S8-S9**), both Vorinostat- and Entinostat-treatment significantly ($p < 0.0001$) reduced monocyte chemoattractant protein-1 (MCP-1; also known as chemokine (C-C motif) ligand 2, CCL2) secretion (Fig. 5**D**). This effect was more pronounced with TNF-α stimulation, as the effect persisted over 24 hrs. Thus, our two HDAC inhibitors appear to have a relatively targeted effect on an inflammatory response, one that involves reduced recruitment of myeloid cells and other leukocytes by MCP-1.

3. Discussion

This report presents an approach to study microglia-like cells that express certain elements of the human DAM signatures in a reproducible fashion. This is essential to enable the functional characterization of this subtype of microglia *in vitro* in a standardized manner over time and across laboratories; functional characterization of primary microglia is impractical with current technologies given the difficulty of accessing a reasonable number of these cells from the human brain. Our *in silico* analyses identified HDAC inhibitors as a class of molecules with the potential to recapitulate aspects of the RNA signatures seen in this subtype of microglia that has been associated with neurodegenerative disease in humans and mice (Friedman, 2018; Green et al., 2024; Keren-Shaul, 2017; Mathys, 2019; Pettas, 2022; Tuddenham, 2024). We prioritized two of these molecules, Vorinostat and Entinostat, and validated our prediction, showing (1) recapitulation of key aspects of the signatures derived from primary human microglia, (2) induction of *MITF*, recently proposed as a regulator of this signature in a study using a different, less reproducible polarization strategy (Dolan et al., 2023), (3) substrate-specific alterations of uptake consistent with the proposed enhanced phagocytic capacity of DAM-enriched cells (Keren-Shaul et al., 2017; Dolan et al., 2023), and (4) a targeted reduction of MCP-1 secretion following TNF-α or IFN-γ stimulation (Fig. 5**E**).

The two HDAC inhibitors – Vorinostat and Entinostat – yield a reproducible model system, that captures aspects of the various murine (DAM1/DAM2[1]) and human (cluster 11[6]) signatures, but its transcriptional effect resembles most closely the recently identified human microglia 13[11] signature that is proposed to mark a microglial subtype contributing to the accumulation of AD pathology (Green et al., 2024). Further, we describe sharing of marker genes and functional changes (increased uptake) with a prior effort to model these signatures *in vitro*

Table 1
List of genes altered in HMC3 cells.

Gene	Signature	Vorinostat treatment FDR [log2FC]	Entinostat treatment FDR [log2FC]
A2M	Cluster 11	*0.117 [3.83]*	0.00368 [6.10]
ACSL1	Cluster 11	*0.066 [0.50]*	3.78E^{-10} [1.49]
ANXA5	Cluster 11	*0.846 [-0.05]*	2.66E^{-09} [0.47]
CALM1	Cluster 11	*0.893 [-0.02]*	3.49E^{-16} [0.85]
CEBPA	Cluster 11	*0.394 [0.44]*	1.46E^{-22} [3.76]
CPM	Cluster 11, Mic13	2.93E^{-15} [2.47]	5.46E^{-41} [4.04]
CTSB	Cluster 11	9.91E^{-19} [0.73]	8.64E^{-35} [0.99]
CTSL	Cluster 11	*0.367 [-0.11]*	2.64E^{-18} [0.86]
CXCL16	Cluster 11	*0.0689 [-0.33]*	0.0401 [0.34]
DBI	Cluster 11	*0.361 [0.12]*	3.00E^{-08} [0.59]
DHRS9	Cluster 11	*0.792 [-0.67]*	0.0036 [4.41]
DRAP1	Cluster 11	3.35E^{-07} [0.53]	*1.78E^{-16} [-0.82]*
FABP5	Cluster 11	0.0416 [0.35]	2.01E^{-43} [2.0]
FTL	Cluster 11	0.0292 [0.44]	*0.525 [0.13]*
GSN	Cluster 11	1.18E^{-38} [2.08]	1.82E^{-49} [2.34]
HTRA1	Cluster 11	2.08E^{-12} [1.93]	1.13E^{-28} [2.92]
LGALS3	Cluster 11	0.00137 [0.35]	4.91E^{-20} [0.9]
LGALS9	Cluster 11	*0.567 [-0.34]*	2.19E^{-10} [2.56]
MT2A	Cluster 11	0.000294 [0.69]	0.0321 [0.40]
PRDX1	Cluster 11	7.76E^{-08} [0.77]	*0.0832 [0.26]*
RAMP1	Cluster 11	*0.631 [-0.22]*	5.04E^{-08} [1.78]
S100A4	Cluster 11	0.00414 [1.17]	0.00768 [1.03]
SDCBP	Cluster 11	0.00845 [0.46]	4.56E^{-23} [1.56]
SLC3A2	Cluster 11	7.58E^{-08} [0.66]	9.21E^{-08} [0.63]
TALDO1	Cluster 11	2.25E^{-06} [0.68]	*0.524 [0.09]*
TYMP	Cluster 11	*0.936 [0.05]*	1.21E^{-05} [1.63]
ADAM28	Mic13	*0.803 [-0.62]*	0.00974 [4.07]
ADAMTS17	Mic13	0.0331 [2.20]	6.46E^{-08} [4.81]
ADARB1	Mic13	2.14E^{-33} [1.18]	6.03E^{-21} [0.92]
ADK	Mic13	*0.241 [-0.15]*	0.0118 [0.27]
ASAH1	Mic13, Cluster 11	0.0113 [0.68]	4.28E^{-08} [1.34]
CADM1	Mic13	1.16E^{-06} [0.48]	1.62E^{-25} [0.96]
CD83	Mic13	*0.337 [0.25]*	1.57E^{-09} [1.25]
CHSY3	Mic13	*0.118 [1.14]*	8.83E^{-07} [2.97]
CPED1	Mic13	6.13E^{-09} [1.21]	6.92E^{-39} [2.49]
CSGALNACT1	Mic13	7.85E^{-11} [2.24]	9.21E-^{16} [2.65]
CTTNBP2	Mic13	*0.932 [-0.23]*	0.000486 [5.09]
CYTH3	Mic13	1.25E^{-08} [0.744]	4.40E^{-23} [1.23]
DENND4C	Mic13	*0.742 [0.07]*	0.0063 [0.41]
DPYD	Mic13	4.10E^{-09} [1.21]	1.32E^{-14} [1.52]
DSCAM	Mic13	*0.718 [1.2]*	0.00123 [6.80]
DTNA	Mic13	1.06 E^{-04} [1.14]	7.44E^{-17} [2.23]
ELMO1	Mic13	*0.0699 [1.95]*	5.40E^{-08} [4.96]
EPB41L3	Mic13	0.0264 [1.49]	0.000111 [2.33]
FAM13A	Mic13	*0.0936 [0.554]*	0.00869 [0.78]
FLT1	Mic13	1.00E^{-07} [2.07]	1.01E^{-30} [4.13]
FMNL2	Mic13	5.42E^{-06} [0.94]	8.03E^{-16} [1.56]
FRMD4B	Mic13	0.0443 [0.63]	0.000321 [1.01]
GAS7	Mic13	8.25 E^{-04} [0.49]	1.90E^{-23} [1.33]
GPNMB	Mic13, Cluster 11	*0.717 [0.58]*	0.00104 [3.59]
HDAC9	Mic13	6.79 E^{-04} [1.20]	3.78E^{-12} [2.25]
IL6ST	Mic13	1.17E^{-05} [0.52]	5.07E^{-11} [0.74]
ITPR2	Mic13	*0.426 [0.29]*	1.83E^{-07} [1.47]
LIPA	Mic13, Cluster 11	2.25E^{-07} [1.22]	5.68E^{-1} [1.48]
MAF	Mic13	*0.131 [1.38]*	3.61E^{-06} [3.57]
MAFB	Mic13, Cluster 11	*0.515 [0.63]*	2.47E^{-09} [4.31]
MITF	Mic13	9.01E^{-28} [1.35]	1.19E^{-23} [1.23]
MSR1	Mic13, Cluster 11	*0.282 [1.66]*	0.0445 [2.65]
MTSS1	Mic13	7.01E^{-06} [1.22]	6.90E^{-25} [2.58]
NAMPT	Mic13	0.0378 [0.26]	1.14E^{-06} [0.55]
NCK2	Mic13	*0.299 [-0.16]*	2.36E^{-10} [0.79]
NPL	Mic13, Cluster 11	*0.333 [1.0]*	5.98E^{-07} [4.02]
PADI2	Mic13, Cluster 11	3.69E^{-36} [3.87]	2.97E^{-78} [5.66]
PDE3B	Mic13	*0.153 [1.15]*	3.16E^{-05} [2.82]
PICALM	Mic13	0.0183 [0.30]	*0.499 [0.08]*
PPARG	Mic13	0.0231 [0.66]	*0.104 [0.45]*
PREX1	Mic13	1.70E^{-07} [1.32]	1.86E^{-21} [2.27]
RALGAPA2	Mic13	0.0262 [0.73]	1.42E^{-10} [1.88]
RASGEF1B	Mic13	*0.444 [0.70]*	0.00105 [2.35]
RASGEF1C	Mic13	*0.983 [0.02]*	3.03E^{-07} [2.84]
RGCC	Mic13, Cluster 11	0.016 [1.59]	2.48E^{-06} [2.77]
SCIN	Mic13, Cluster 11	1.56E^{-05} [1.47]	4.79E^{-32} [3.57]
SDK1	Mic13	*0.202 [0.19]*	7.06E^{-24} [1.20]
SERPINB9	Mic13	0.00244 [1.79]	1.93E^{-12} [3.75]
SLC1A3	Mic13	0.00338 [0.47]	4.61E^{-08} [0.80]
SLC9A9	Mic13	*0.117 [1.44]*	0.0215 [1.88]
SRGAP1	Mic13	*0.107 [0.24]*	0.0411 [0.28]
SRGAP2	Mic13	0.00118 [0.62]	0.000226 [0.66]
SRGAP2B	Mic13	*0.215 [0.17]*	0.00138 [0.38]
SSBP2	Mic13	0.00121 [0.94]	0.007 [0.75]
ST6GALNAC3	Mic13	0.0207 [2.36]	2.20E^{-10} [5.67]
SYNDIG	Mic13	*0.719 [1.21]*	0.00149 [6.75]
TANC2	Mic13	9.03E^{-13} [0.65]	0.000168 [0.34]
TBXAS1	Mic13	0.0806 [0.85]	0.00713 [1.17]
TLN2	Mic13	1.46E^{-10} [1.66]	1.89E^{-36} [3.10]
TMEM163	Mic13	2.97E^{-05} [2.6]	3.01E^{-12} [4.01]
WIPF3	Mic13	*0.923 [0.12]*	6.07E^{-06} [3.17]
XYLT1	Mic13	*0.69 [1.2]*	0.0425 [4.42]
CADM1	DAM1/2	1.16E^{-06} [0.48]	1.62E^{-25} [0.96]
CD52	DAM1/2	0.0149 [1.66]	2.72E^{-05} [2.56]
CD9	DAM1/2, Cluster 11	5.16E^{-49} [1.41]	3.47E^{-100} [2.00]
CST7	DAM1/2	*0.633 [0.65]*	5.74E^{-10} [5.28]
CTSL	DAM1/2	*0.367 [-0.11]*	2.64E^{-18} [0.86]
GUSB	DAM1/2	*0.937 [0.01]*	1.11E^{-07} [0.72]
HIF1A	DAM1/2	*0.01 [-0.21]*	2.71E^{-11} [0.51]
ITGAX	DAM1/2, Mic13, Cluster 11	7.90E^{-15} [3.04]	1.12E^{-34} [4.57]
LPL	DAM1/2, Mic13, Cluster 11	0.00325 [4.75]	1.41E^{-13} [10.4]
SPP1	DAM1/2, Cluster 11	8.65E^{-07} [3.94]	2.39E^{-20} [6.85]
APOE	DAM1/2, Mic13, Cluster 11	0.0012 [1.13]	4.30E^{-07} [1.61]
B2M	DAM1/2	2.16E^{-11} [0.56]	5.77E^{-17} [0.68]
CTSB	DAM1/2	9.91E^{-19} [0.73]	8.64E^{-35} [0.99]
FTH1	DAM1/2, Cluster 11	0.0026 [0.29]	5.62E^{-05} [0.36]
TIMP2	DAM1/2	1.58E^{-07} [0.64]	1.57E^{-07} [0.62]

Summary of all signature genes induced by Vorinostat and/or Entinostat in HMC3 microglia-like cells. Italics indicate results of non-significance or negative regulation. Mic13 = microglia 13 signature (Green et al., 2024).

using apoptotic neurons among other substrates as a polarizing agent in iMG to yield a DAM-like phenotype (Dolan et al., 2023). We therefore have addressed the challenge of reproducibility that is intrinsic to the use of cell-preparation derived reagents. In addition, Vorinostat and Entinostat are well-characterized tool compounds that can serve as reference molecular structures for further optimization of desired compound characteristics. Moreover, Vorinostat is approved by the Federal Drug Administration for the treatment of cutaneous T cell lymphoma (Olsen et al., 2007), facilitating translation to human study participants.

Our study has certain limitations; first, given the difficulty of accessing primary human microglia, we used cellular model systems in our experiments. The use of two distinct human microglia-like models – the HMC3 cell line and iMG – mitigates this limitation: the two model systems are complementary and provide consistent results for a subset of DAM-like signature genes. Further, since the original DAM signature (Keren-Shaul et al., 2017) is derived from mice and there is no single, generally accepted human DAM signature, we elected to evaluate multiple different signatures that are overlapping. The use of both scRNA-seq- (cluster 11) (Tuddenham et al., 2024) and snRNAseq- (microglia 13) (Green et al., 2024) derived signatures helps to address the concern that the type of single cell preparation (living cell vs. nucleus isolation) could influence the nature of the signature. Our characterization so far clearly suggests that, while HDAC inhibitors may engage some key DAM genes, they do not recapitulate the entire signature; additional compounds may be needed to achieve the full reconstitution of the signature. Nonetheless, HDAC inhibitors offer an entry point into DAM biology that needs to be investigated further.

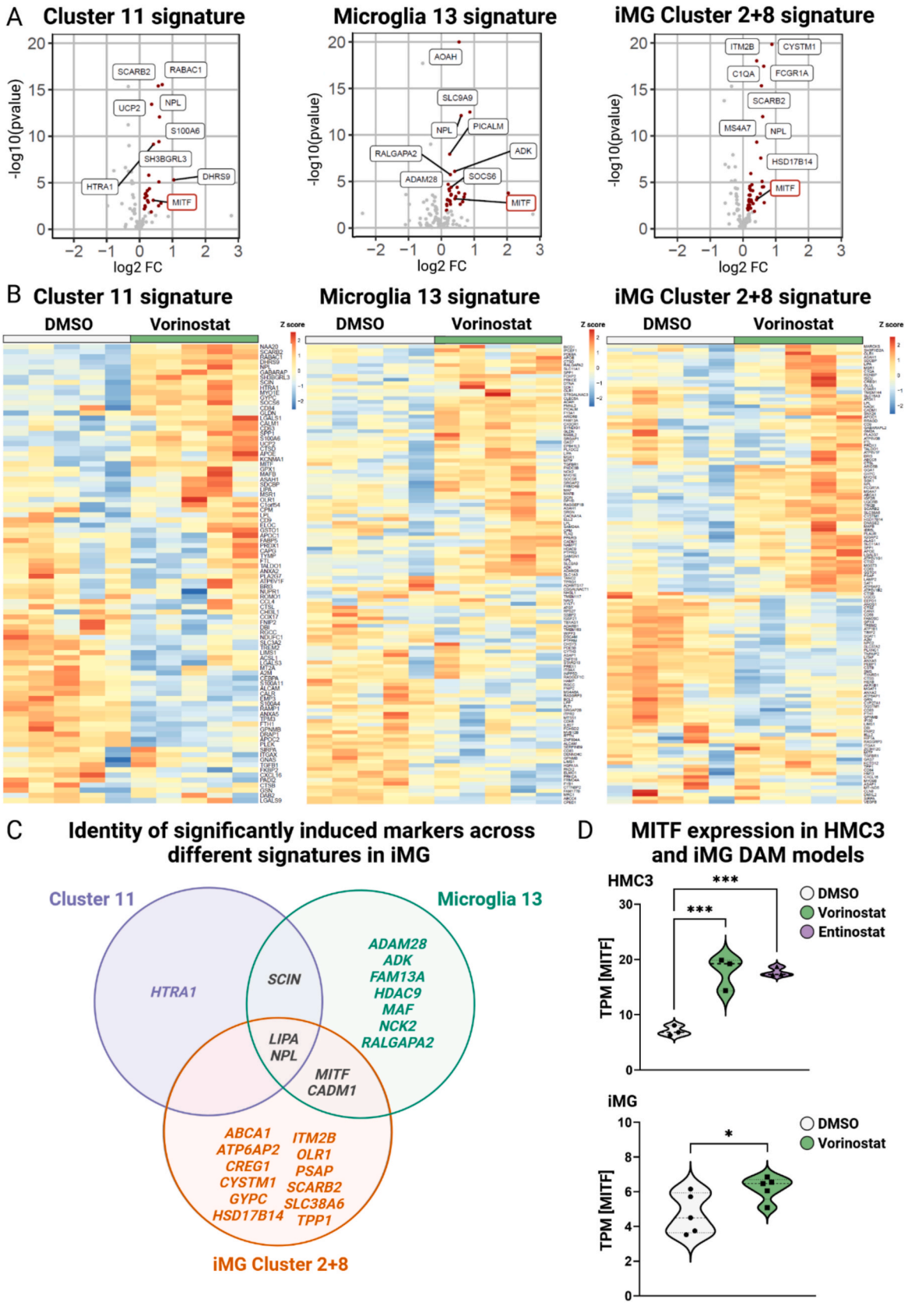

(caption on next page)

Fig. 4. Bulk RNA-Seq of the human iPSC-derived microglia (iMG) DAM model. **A. Volcano Plots depicting the distribution of differentially expressed genes from different signatures (Cluster 11[6], Microglia 13[11], iMG Cluster 2 + 8[9]) for Vorinostat treatment in comparison to DMSO control.** iPSC-derived microglia at Day 28–29 of differentiation were treated for 24hrs with DMSO as control (1:100.000) or Vorinostat (0.1 μM) and were profiled using bulk RNAseq. Volcano plots depict all genes present in each marker set (Cluster 11[6]: 89 genes, Microglia 13[11]: 127 genes, iMG Cluster 2 + 8 (Dolan et al., 2023): 134 genes) plotted based on log2 fold change (FC) expression and −log10(p value) with the ones significantly upregulated marked in red and, of the most significantly changed genes, a selection of nine genes was labeled with the gene name. Plots are organized from Cluster 11 (left)[6], to Microglia 13 (middle)[11], to iMG Cluster 2 + 8 (right)[9]. **B. Heatmaps showing the expression of Cluster 11[6]** (left), **Microglia 13[11]** (middle) and iMG Cluster 2 + 8[9] (right) **marker sets** in bulk RNAseq data generated 24hrs following compound treatment with DMSO (control; 1:10.000; white) or Vorinostat (green; 0.1 μM). Each column represents a single sample, each row a single gene represented in the respective marker set. Pairwise differential testing between DMSO control and each of the treatment conditions (DMSO control, 1:10.000; Vorinostat, 1 μM) was conducted using a Wald test with the Benjamini-Hochberg correction (FDR alpha < 0.05). The legend represents Z scores, with lower scores indicated in red and higher scores indicated in blue. Data represents n = 5 independent experiments per treatment group from one differentiation of iPSC-derived human microglia. For data replication in a second differentiation see Supple. Fig. 4. **C. Venn diagram depicting significantly induced markers across the signatures for Cluster 11[6], Microglia 13[11] and iMG Cluster 2 + 8[9] in Vorinostat-treated iMGs.** Each circle shows significantly induced markers from each marker set – Cluster 11[6] (violet), Microglia 13 (green)[11], iMG Cluster 2 + 8[9] (orange). Overlays of circles depict induced marker genes shared across different combinations of marker sets. Percentage indicates ratio of each marker set in relation to the total number of significantly induced markers across all three signatures. **D. MITF expression in HMC3 and iMG DAM models.** Violin plots depict the expression of the transcription factor MITF in transcripts per million (TPM) across treatment conditions in HMC3 microglia (top; DMSO (blue; 1:1000 for Entinostat; 1:10.000 for Vorinostat; white), Vorinostat (1 μM; green), Entinostat (10 μM; purple); n = 3/group) and iMG (bottom; DMSO (white), Vorinostat (0.1 μM; green); n = 6 per group, one iMG differentiation; for data replication see Suppl. Fig. 4). For statistical analysis of HMC3 data, one-way ANOVA followed by Dunnett's multiple comparisons test was performed. For iMG data, unpaired *t*-test was performed. Each dot represents a replicate, central interrupted line represents the median and fine dotted lines represent the interquartile range. *p.adj ≤ 0.05, **p.adj ≤ 0.01, ***p.adj ≤ 0.001 test. (For interpretation of the references to color in this figure legend, the reader is referred to the web version of this article.)

Moreover, while RNA signatures provide a very useful entry into the characterization of a putative cell subtype or state, they are limited in their ability to guide further functional studies; therefore, the next generation of model systems will require validation at the protein level. This is currently limited by the availability of human datasets defining microglial subsets at the protein level. Second, a signature may define a cell state, but it can be composed of distinct transcriptional programs that co-occur in a certain context. This is well-described for response to Type I interferons (Mostafavi et al., 2016), in which at least 5 transcriptional programs can be resolved. Our data suggest that this is also the case for the DAM signatures, as in the context of two different model systems (HMC3 and iMG) and Entinostat or Vorinostat exposure – illustrated in Fig. 3**A/4B** – there are at least two distinct subgroups of genes present in each of the signatures. The HDAC inhibitors engage one of these and appear to reduce expression of the other, smaller subgroup of genes that appears to be upregulated in the baseline state of these *in vitro* model systems in which microglia-like cells are likely to be somewhat activated. Further work will be needed to understand the role of each of these two gene subgroups. The larger subgroup, which is expressed at higher levels following exposure to HDAC inhibitors contains most of the key markers that the community has used to define the DAM signatures. This subgroup also contains *MITF* which is a transcriptional factor that has been recently proposed as a regulator of the iMG DAM Clusters 2 + 8 (Dolan et al., 2023). *MITF* expression is enhanced in both of our model systems (HMC3 microglia and iMG) following HDAC inhibitor treatment (Fig. 4**D**). Whether our functional observations are *MITF*-dependent was not further investigated in our context, as on the one hand the proposed MITF pathway inhibitor ML329 has previously been shown to significantly reduce Aβ phagocytosis in iMG (Lee et al., 2024) and, on the other hand, a review of the ML329 literature returns no description of its mechanism. It is not known to bind MITF; it was discovered in a high-throughput phenotypic screen for compounds altering the promoter activity of melastatin (TRPM1) in the MITF-dependent melanoma cell line SK-MEL-5 (Faloon et al., 2010). Its role as a MITF inhibitor was inferred but not demonstrated (Faloon et al., 2010).

The authors of the study reporting the role of MITF highlight *ABCA1*, *APOE*, *GPNMB*, *LPL* and *TREM2* as key markers that overlap between their iPSC-derived DAM model and human brain biopsy samples when integrated into their dataset (Dolan et al., 2023). Interestingly, in our model systems, we also observed a significant increase of *ABCA1*, *APOE*, *LPL*, further confirming their results (Table 2, **Table S3**). The third challenge of studying RNA-defined cell subsets involves the relation of RNA signatures, which are very dynamic, to cellular function. Our data illustrate this in that Entinostat appears to have a very strong effect on the RNA signatures when compared to Vorinostat, but Vorinostat has the stronger effect when it comes to pHrodoDextran and Aβ1-42 uptake (Fig. 5**A-B**). This illustrates the limitation of RNA-based signatures in studying cellular functions such as Aβ1-42 uptake that may be the more clinically relevant outcome measure. Nonetheless, the DAM signatures were critical to the prioritization of these tool compounds.

The current literature on human DAM or DAM-like states does not provide any comprehensive information on whether microglia have to transition through the DAM1 state in order to become DAM2. In fact, until recently, it was not clear whether DAM or DAM-like states existed among human microglia (Mathys et al., 2019; Sobue et al., 2021; Srinivasan et al., 2020). Driven by technological advances, novel, emerging datasets all support the existence of DAM-like states in humans (Tuddenham et al., 2024; Green et al., 2024; Gerrits et al., 2021; Smith et al., 2022; Gazestani et al., 2023). In our analysis of our sc- and snRNAseq datasets with regards to DAM1 and DAM2 signature expression (Keren-Shaul et al., 2017), we observed microglia with DAM2-specific expression to be focused to regions that also showed a high expression in DAM1 marker genes, suggesting that DAM2 might arise from DAM1, but that not all microglia might transition from a DAM1 to a DAM2 state. In fact, the average proportion of DAM2 microglia is ~1 % (Tuddenham et al., 2024) of all microglia in older individuals (Fig. 1**C-D**). On the other hand, as DAM1 marker expression is spread across almost half of our scRNAseq (Tuddenham et al., 2024) dataset, DAM1 may represent an aging- or senescence- associated microglial cluster, supported by the high expression of *CSTB* and *TIMP2* which have also been proposed as markers for senescent microglia (Saul et al., 2022; Zhao et al., 2022). The live primary human microglia profiled in this study also undergo more manipulation (the effect of which is minimized by keeping the experimental pipeline on ice) than the nuclei derived from flash-frozen tissue, and this may contribute to some of the observed DAM1 changes. Similarly, whether DAM represent a subtype of microglia or rather a state of reaction as result of a changed microenvironment

Table 2
List of genes altered in iMG.

Gene	Signature	Entinostat HMC3 FDR [log2FC]	Vorinostat HMC3 FDR [log2FC]	Vorinostat iMG D1: FDR [log2FC] D2: FDR [log2FC]
HTRA1	Cluster 11	1.13E^{-28} [2.92]	2.08E^{-12} [1.93]	D1: 1.83E^{-08} [0.41] D2: 9.37E^{-07} [0.66]
LIPA	Cluster 11, Mic13, iMG 2 + 8	5.68E^{-11} [1.48]	2.2.5E^{-07} [1.22]	D1: 5.92E^{-04} [0.23] D2: *0.0675 [0.97]*
NPL	Cluster 11, Mic13, iMG 2 + 8	5.98E^{-07} [4.02]	*0.333 [1.0]*	D1: 3.37E^{-11} [0.60] D2: 0.00059 [0.75]
SCIN	Cluster 11, Mic13	4.79E^{-32} [3.57]	1.56E^{-05} [1.47]	D1: 1.40E^{-02} [0.58] D2: 0.012 [1.04]
ADAM28	Mic13	0.00974 [4.07]	*0.803 [-0.62]*	D1: 0.000208 [0.21] D2: 1.78E^{-07} [0.79]
ADK	Mic13	0.0118 [0.27]	*0.241 [-0.15]*	D1: 1.17E^{-05} [0.41] D2: *0.0553 [0.46]*
CADM1	Mic13, iMG 2 + 8, DAM1/2	1.62E^{-25} [0.96]	1.16E^{-06} [0.48]	D1: 5.72E^{-03} [0.18] D2: 0.00171 [0.53]
FAM13A	Mic13	0.00869 [0.779]	*0.0936 [0.554]*	D1: 0.00168 [0.71] D2: 0.0165 [0.98]
HDAC9	Mic13	3.78E^{-12} [2.25]	0.000679 [1.2]	D1: 0.048 [0.16] D2: 1.76E^{-15} [1.56]
MAF	Mic13	3.61E^{-06} [3.57]	*0.131 [1.38]*	D1: 0.000839 [0.25] D2: 0.000575 [0.54]
MITF	Mic13, iMG 2 + 8	1.19E^{-23} [1.23]	9.01E^{-28} [1.35]	D1: 0.00452 [0.41]D2: 0.000588 [0.95]
NCK2	Mic13	2.36E^{-10} [0.79]	*0.299 [-0.16]*	D1: 0.0138 [0.28] D2: *0.131 [0.37]*
RALGAPA2	Mic13	1.42E^{-10} [1.88]	0.0262 [0.73]	D1: 2.41E^{-05} [0.27] D2: *0.115 [0.33]*
APOE	DAM1/2, Mic13, Cluster 11	4.30E^{-07} [1.61]	0.0012 [1.13]	D1: *0.345 [0.38]* D2: 0.00136 [2.42]
LPL	DAM1/2, Mic13, Cluster 11	1.41E^{-13} [10.4]	0.00325 [4.75]	D1: *0.894 [0.05]* D2: 8.17E^{-06} [1.46]
ABCA1	iMG 2 + 8	n/a	n/a	D1: 0.000283 [0.63] D2: 3.05E^{-06} [1.77]
ATP6AP2	iMG 2 + 8	n/a	n/a	D1: 0.00173 [0.19] D2: 0.025 [0.36]
CREG1	iMG 2 + 8	n/a	n/a	D1: 0.00018 [0.28] D2: 0.0121 [0.49]
CYSTM1	iMG 2 + 8	n/a	n/a	D1: 1.55E^{-18} [0.88] D2: 8.91E^{-09} [1.40]
GYPC	iMG 2 + 8	n/a	n/a	D1: 8.78E^{-05} [0.58] D2: 7.03E^{-05} [0.94]
HSD17B14	iMG 2 + 8	n/a	n/a	D1: 4.61E^{-07} [0.54] D2: 3.49E^{-11} [1.34]
ITM2B	iMG 2 + 8	n/a	n/a	D1: 1.03E^{-17} [0.40] D2: 3.67E^{-1}0 [0.86]
OLR1	iMG 2 + 8	n/a	n/a	D1: 0.0141 [0.16] D2: 0.000308 [0.54]
PSAP	iMG 2 + 8	n/a	n/a	D1: 0.0362 [0.16] D2: 0.0151 [0.42]
SCARB2	iMG 2 + 8	n/a	n/a	D1: 2.43E^{-14} [0.56] D2: 6.66E^{-05} [0.68]
SLC38A6	iMG 2 + 8	n/a	n/a	D1: 0.000296 [0.59] D2: 2.68E^{-05} [1.26]
TPP1	iMG 2 + 8	n/a	n/a	D1: 0.0265 [0.14] D2: 0.0191 [0.38]

Summary of top marker genes induced by both compounds in HMC3 and two independent differentiations of iMG (only Vorinostat-treated; D1 = differentiation 1; D2 = differentiation 2). Italics indicate results of non-significance or negative regulation. Mic13 = microglia 13 signature (Green et al., 2024).

remains to be further defined and discussed by the community (Stratoulias et al., 2019).

Our *in silico* analyses (Fig. 2**A-B, Fig. S2A**) prioritized a broad range of compounds with HDAC inhibition properties. Our subsequent transcriptomic and functional studies following Vorinostat and Entinostat exposure have validated this initial observation. This report joins a growing literature implicating HDAC activity in neurodegeneration and in microglial function in particular. For example, HDAC inhibition has been suggested to perturb the state of microglial activation (Suuronen et al., 2003) and to cause functional changes, including suppression of cytokine and chemokine (Kuboyama et al., 2017) secretion. Further, ablation of HDAC1/HDAC2 in mice is reported to enhance microglial amyloid phagocytosis and to decrease amyloid load in an amyloid proteinopathy model (Datta et al., 2018). Additionally, HDAC2 is implicated in the negative regulation of memory and synaptic plasticity and has been reported to be increased in postmortem samples from AD patients (Guan et al., 2009; Gräff et al., 2012). Finally, HDAC6 has been reported to be increased in postmortem samples from individuals with AD and may be involved in metabolism of tau (Ding et al., 2008).

Aside from enhanced Aβ 1–42 uptake which is consistent with previous reports of the *MITF*-dependent DAM model that has enhanced phagocytosis (Dolan et al., 2023), our functional analyses also yielded a specific downregulation of TNFα- or IFNy-induced MCP-1 secretion in both Vorinostat- and Entinostat- treated cells. MCP-1 has emerged as a cytokine with pivotal roles in many CNS disorders: it is present in senile amyloid plaques and reactive microglia in AD (summarized in (Singh et al., 2022). Moreover, elevated MCP-1 serum levels are increased in mild cognitive impairment (MCI) as well as in mild AD (Galimberti et al., 2006). Additionally, in cerebrospinal fluid (CSF), MCP-1 levels are significantly increased and positively correlated with phosphorylated tau and ß-amyloid levels (Corrêa et al., 2011). Thus, microglia enriched in DAM-related signatures may be having multiple effects in AD, reducing Aβ1-42 load and possibly reducing leukocyte recruitment, rather implying a beneficial than detrimental role in neurodegeneration; however, further studies are needed to address these hypotheses.

The development of model systems with which to study human DAM physiology and function bears great potential. Here, we have presented an initial foray into *in silico* prioritization of tool compounds that successfully predicted HDAC inhibitors as tool compounds that engage a key DAM regulator, *MITF*. They present an interesting lead to pursue in

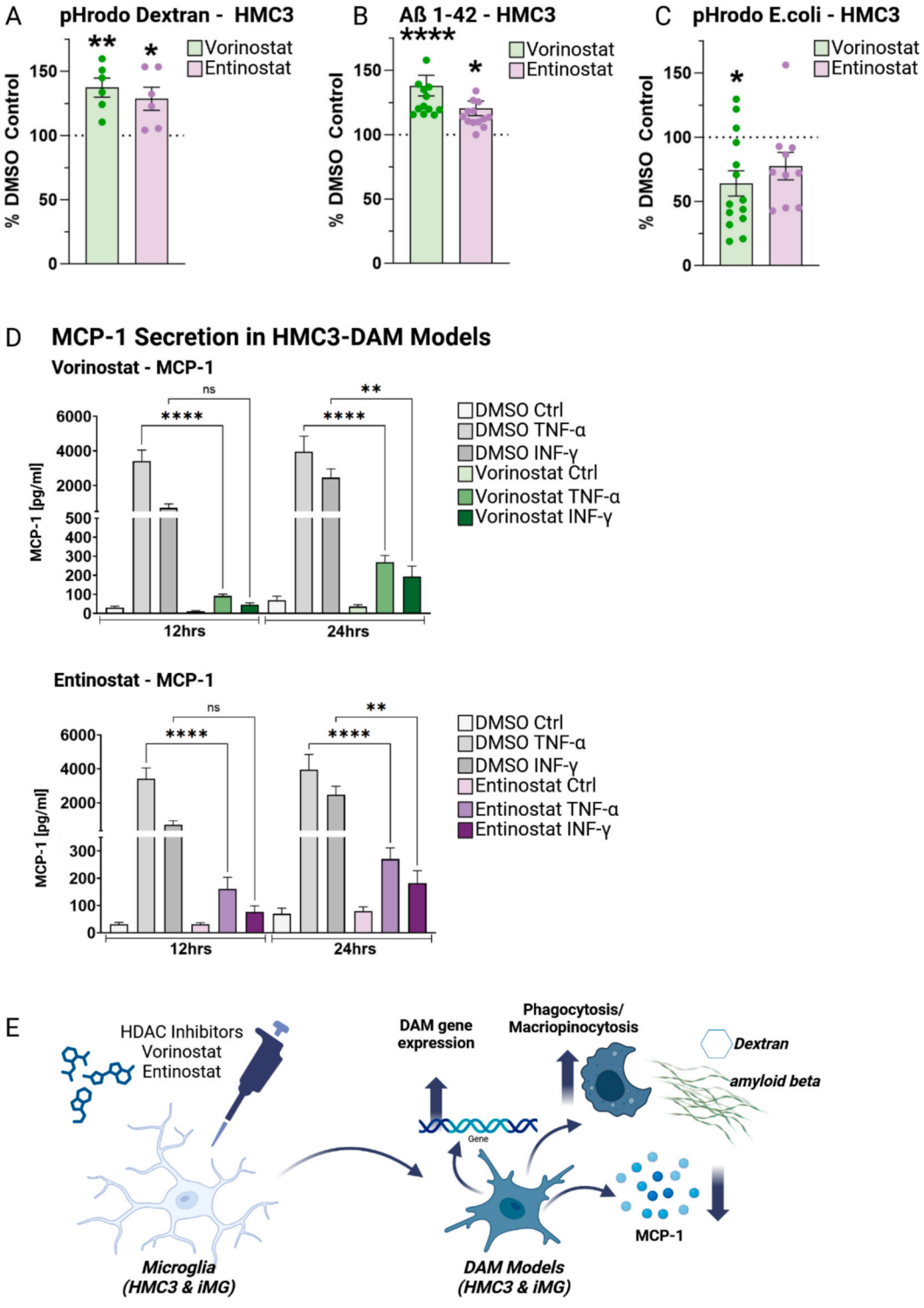

(caption on next page)

Fig. 5. Compound-treated HMC3 microglia exhibit substrate-specific endocytic and phagocytic phenotypes as well as differences in secretion of pro-inflammatory cytokines. **A. Vorinostat and Entinostat upregulate pHrodoDextran phagocytosis.** HCM3 microglia-like cells were pretreated each compound or DMSO as control for 24hrs. Subsequently, they were exposed to pHrodo-labeled Dextran for 1hr, and the uptake of pHrodo-labeled Dextran was assessed using flow cytometry. Individual experiments are depicted as individual dots in the bar graphs depicting mean ± SEM (Vorinostat – green; Entinostat– purple). Phagocytosis was normalized to percent DMSO (% DMSO) control and for statistical analysis, log-fold change values in comparison to DMSO-treated control samples were analyzed using one-way ANOVA followed by Dunnett's multiple comparison test. *p.adj ≤ 0.05; **p.adj ≤ 0.01. **B. Vorinostat and Entinostat induce Aß1-42 phagocytosis in HMC3 microglia-like cells.** HCM3 microglia were pretreated with each compound or DMSO as control for 24hrs, subsequently exposed to AlexaFluor 647-labeled Aß monomers for 1hr and subsequently the uptake of AlexaFluor 647-labeled Aß monomers was assessed using flow cytometry Individual experiments are depicted as individual dots in the bar graphs depicting mean ± SEM (Vorinostat – green; Entinostat – purple). Phagocytosis was normalized to % DMSO control and for statistical analysis, log-fold change values in comparison to DMSO-treated control samples were analyzed using one-way ANOVA followed by Dunnett's multiple comparison test. *p.adj ≤ 0.05; ** p.adj ≤ 0.01. **C. Vorinostat reduces phagocytosis of pHrodo-labeled E.coli.** HCM3 microglia-like cells were pretreated with each compound or DMSO as control for 24hrs, exposed to pHrodo-labeled E.coli particles (1hr) and the uptake of pHrodo-labeled E.coli particles was assessed using flow cytometry. Individual experiments are depicted as individual dots in the bar graphs depicting mean ± SEM (Vorinostat – green; Entinostat – purple). Phagocytosis was normalized to % DMSO control and for statistical analysis, log-fold change values in comparison to DMSO-treated control samples were analyzed using one-way ANOVA followed by Dunnett's multiple comparison test. *p.adj ≤ 0.05; **p.adj ≤ 0.01. **D. Vorinostat and Entinostat, decrease the secretion of pro-inflammatory cytokine MCP-1.** HMC3 microglia-like cells were pre-treated with Vorinostat or Entinostat for 24hrs, and subsequently stimulated with either TNF-α (0.3 μg/mL), IFN-γ (0.3 μg/mL) or H_2O as control for 12 or 24 hrs. Supernatant was collected and MCP-1 secretion assessed using a human pro-inflammatory cytokine discovery assay. Bargraphs depict measured amount of MCP-1 (mean ± SEM) in pg/ml for DMSO control-treated samples (white, light gray, gray) or compound-treated samples (light green, green dark green (Vorinostat)/light purple, purple, dark purple (Entinostat)). For statistical analysis, one-way ANOVA followed by Tukey's multiple comparisons test with a single pooled variance was performed. *p.adj ≤ 0.05; **p.adj ≤ 0.01; ***p.adj ≤ 0.001; ****p.adj ≤ 0.0001. **E. Summary graph** depicting overall results from this study. (For interpretation of the references to color in this figure legend, the reader is referred to the web version of this article.)

the development of immunomodulatory agents that can deployed *in vivo*, to resolve the question of whether DAMs should be enhanced or suppressed in the context of AD.

CRediT authorship contribution statement

Verena Haage: Writing – original draft, Visualization, Validation, Supervision, Project administration, Methodology, Investigation, Formal analysis, Data curation, Conceptualization. **John F. Tuddenham:** Writing – review & editing, Visualization, Methodology, Investigation, Formal analysis, Data curation, Conceptualization. **Alex Bautista:** Validation, Methodology, Investigation, Formal analysis, Data curation. **Frankie Garcia G.:** Validation, Investigation, Formal analysis. **Charles C. White:** Visualization, Software, Formal analysis, Data curation. **Ronak Patel:** Validation, Methodology. **Natacha Comandante-Lou:** Formal analysis. **Victoria Marshe:** Formal analysis. **Jennifer Griffin:** Investigation, Writing – review & editing. **Ye Zhou:** Investigation, Writing – review & editing. **Deniz Ghaffari:** Investigation, Writing – review & editing. **Beatrice Acheson:** Investigation, Writing – review & editing. **Mariko Taga:** Investigation, Writing – original draft, Writing – review & editing. **Peter H. St George-Hyslop:** Investigation, Writing – review & editing. **Rajesh Kumar Soni:** Methodology, Data curation. **Peter A. Sims:** Supervision. **Vilas Menon:** Supervision. **Andrew A. Sproul:** Supervision, Resources, Methodology. **Philip L. De Jager:** Writing – original draft, Writing – review & editing, Supervision, Resources, Project administration, Methodology, Funding acquisition, Conceptualization.

Declaration of competing interest

The authors declare that they have no known competing financial interests or personal relationships that could have appeared to influence the work reported in this paper.

Acknowledgements

The work was supported by the Chan-Zuckerberg Initiative's Neurodegeneration Challenge Network grant CS-02018-191971. Some of the work also emerged from support from NIH/NIA grants R01 AG070438, U01 AG061356, RF1 AG057473, R01AG048015. Research reported in this publication was supported by the National Institute of General Medical Sciences of the National Institutes of Health under Award Number T32GM007367 and by the National Cancer Institute of the National Institutes of Health under Award Number F30CA261090. AAS is supported by The Thompson Foundation (TAME-AD) and the Henry and Marilyn Taub Foundation.

Research reported in this publication was partially performed in the Columbia Center for Translational Immunology and P&S Flow Cytometry Core and the Sulzberger Genome Center at Columbia University. This research was funded in part through the NIH/NCI Cancer Center Support Grant P30CA013696 and used the Genomics and High Throughput Screening Shared Resource. Moreover, this study used the Confocal and Specialized Microscopy Shared Resource of the Herbert Irving Comprehensive Cancer Center at Columbia University, funded in part through NIH/NCI Cancer Center Support Grant P30CA013696.

All illustrations were created with BioRender.com.

Materials Availability statement

This study did not generate new unique reagents.

Data and Code Availability statement

Sequencing and all other raw data reported in this paper are currently being deposited in the AD knowledge portal.

Appendix A. Supplementary data

Supplementary data to this article can be found online at https://doi.org/10.1016/j.bbi.2025.05.027.

Data availability

Data will be made available on request.

References

Abud, E.M., et al., 2017. iPSC-derived human microglia-like cells to study neurological diseases. Neuron 94, 278–293.e279. https://doi.org/10.1016/j.neuron.2017.03.042.

Asaga, H., Ishigami, A., 2007. Microglial expression of peptidylarginine deiminase 2 in the prenatal rat brain. Cell. Mol. Biol. Lett. 12, 536–544. https://doi.org/10.2478/s11658-007-0025-y.

Butovsky, O., Weiner, H.L., 2018. Microglial signatures and their role in health and disease. Nat. Rev. Neurosci. 19, 622–635. https://doi.org/10.1038/s41583-018-0057-5.

Cadiz, M.P., et al., 2022. Culture shock: microglial heterogeneity, activation, and disrupted single-cell microglial networks in vitro. Mol. Neurodegener. 17, 26. https://doi.org/10.1186/s13024-022-00531-1.

Corrêa, J.D., Starling, D., Teixeira, A.L., Caramelli, P., Silva, T.A., 2011. Chemokines in CSF of Alzheimer's disease patients. Arq. Neuropsiquiatr. 69, 455–459. https://doi.org/10.1590/s0004-282x2011000400009.
Datta, M., et al., 2018. Histone deacetylases 1 and 2 regulate microglia function during development, homeostasis, and neurodegeneration in a context-dependent manner. Immunity 48, 514–529.e516. https://doi.org/10.1016/j.immuni.2018.02.016.
Ding, H., Dolan, P.J., Johnson, G.V., 2008. Histone deacetylase 6 interacts with the microtubule-associated protein tau. J. Neurochem. 106, 2119–2130. https://doi.org/10.1111/j.1471-4159.2008.05564.x.
Dolan, M.-J., et al., 2023. Exposure of iPSC-derived human microglia to brain substrates enables the generation and manipulation of diverse transcriptional states in vitro. Nat. Immunol. 24, 1382–1390. https://doi.org/10.1038/s41590-023-01558-2.
Eckschlager, T., Plch, J., Stiborova, M., Hrabeta, J., 2017. Histone deacetylase inhibitors as anticancer drugs. Int. J. Mol. Sci. 18. https://doi.org/10.3390/ijms18071414.
Faloon, P.W., et al., 2010. Probe Reports from the NIH Molecular Libraries Program. National Center for Biotechnology Information (US).
Friedman, B.A., et al., 2018. Diverse brain myeloid expression profiles reveal distinct microglial activation states and aspects of Alzheimer's disease not evident in mouse models. Cell Rep. 22, 832–847. https://doi.org/10.1016/j.celrep.2017.12.066.
Galimberti, D., et al., 2006. Serum MCP-1 levels are increased in mild cognitive impairment and mild Alzheimer's disease. Neurobiol. Aging 27, 1763–1768. https://doi.org/10.1016/j.neurobiolaging.2005.10.007.
Gazestani, V., et al., 2023. Early Alzheimer's disease pathology in human cortex involves transient cell states. Cell 186, 4438–4453.e4423. https://doi.org/10.1016/j.cell.2023.08.005.
Gerrits, E., et al., 2021. Distinct amyloid-β and tau-associated microglia profiles in Alzheimer's disease. Acta Neuropathol. 141, 681–696. https://doi.org/10.1007/s00401-021-02263-w.
Gräff, J., et al., 2012. An epigenetic blockade of cognitive functions in the neurodegenerating brain. Nature 483, 222–226. https://doi.org/10.1038/nature10849.
Green, G.S., et al., 2024. Cellular communities reveal trajectories of brain ageing and Alzheimer's disease. Nature 633, 634–645. https://doi.org/10.1038/s41586-024-07871-6.
Grubman, A., et al., 2021. Transcriptional signature in microglia associated with Aβ plaque phagocytosis. Nat. Commun. 12, 3015. https://doi.org/10.1038/s41467-021-23111-1.
Guan, J.S., et al., 2009. HDAC2 negatively regulates memory formation and synaptic plasticity. Nature 459, 55–60. https://doi.org/10.1038/nature07925.
Haage, V., et al., 2024. A pharmacological toolkit for human microglia identifies Topoisomerase I inhibitors as immunomodulators for Alzheimer's disease, 2024.2002.2006.579103 bioRxiv, 579103. https://doi.org/10.1101/2024.02.06.579103.
Hasselmann, J., Blurton-Jones, M., 2020. Human iPSC-derived microglia: A growing toolset to study the brain's innate immune cells. Glia 68, 721–739. https://doi.org/10.1002/glia.23781.
Jauregui, C., et al., 2023. Exploring the disease-associated microglia state in amyotrophic lateral sclerosis. Biomedicines 11. https://doi.org/10.3390/biomedicines11112994.
Kannan, V., et al., 2013. Histone deacetylase inhibitors suppress immune activation in primary mouse microglia. J. Neurosci. Res. 91, 1133–1142. https://doi.org/10.1002/jnr.23221.
Keren-Shaul, H., et al., 2017. A unique microglia type associated with restricting development of Alzheimer's disease. Cell 169, 1276–1290.e1217. https://doi.org/10.1016/j.cell.2017.05.018.
Kuboyama, T., et al., 2017. HDAC3 inhibition ameliorates spinal cord injury by immunomodulation. Sci. Rep. 7, 8641. https://doi.org/10.1038/s41598-017-08535-4.
Lee, D., et al., 2024. Plasticity of human microglia and brain perivascular macrophages in aging and Alzheimer's disease. medRxiv. https://doi.org/10.1101/2023.10.25.23297558.
Love, M.I., Huber, W., Anders, S., 2014. Moderated estimation of fold change and dispersion for RNA-seq data with DESeq2. Genome Biol. 15, 550. https://doi.org/10.1186/s13059-014-0550-8.
Maguire, E., et al., 2022. Assaying microglia functions in vitro. Cells 11. https://doi.org/10.3390/cells11213414.
Mathys, H., et al., 2019. Single-cell transcriptomic analysis of Alzheimer's disease. Nature 570, 332–337. https://doi.org/10.1038/s41586-019-1195-2.
McQuade, A., et al., 2018. Development and validation of a simplified method to generate human microglia from pluripotent stem cells. Mol. Neurodegener. 13, 67. https://doi.org/10.1186/s13024-018-0297-x.
Mostafavi, S., et al., 2016. Parsing the interferon transcriptional network and its disease associations. Cell 164, 564–578. https://doi.org/10.1016/j.cell.2015.12.032.
Nakanishi, H., 2020. Microglial cathepsin B as a key driver of inflammatory brain diseases and brain aging. Neural Regen. Res. 15, 25–29. https://doi.org/10.4103/1673-5374.264444.
Olsen, E.A., et al., 2007. Phase IIb multicenter trial of vorinostat in patients with persistent, progressive, or treatment refractory cutaneous T-cell lymphoma. J. Clin. Oncol. 25, 3109–3115. https://doi.org/10.1200/jco.2006.10.2434.
Pettas, S., et al., 2022. Profiling microglia through single-cell RNA sequencing over the course of development, aging, and disease. Cells 11. https://doi.org/10.3390/cells11152383.
Saul, D., et al., 2022. A new gene set identifies senescent cells and predicts senescence-associated pathways across tissues. Nat. Commun. 13, 4827. https://doi.org/10.1038/s41467-022-32552-1.
Shukla, S., Tekwani, B.L., 2020. Histone deacetylases inhibitors in neurodegenerative diseases, neuroprotection and neuronal differentiation. Front. Pharmacol. 11, 537. https://doi.org/10.3389/fphar.2020.00537.
Singh, N., Das, B., Zhou, J., Hu, X., Yan, R., 2022. Targeted BACE-1 inhibition in microglia enhances amyloid clearance and improved cognitive performance. Sci. Adv. 8, eabo3610. https://doi.org/10.1126/sciadv.abo3610.
Smith, A.M., et al., 2022. Diverse human astrocyte and microglial transcriptional responses to Alzheimer's pathology. Acta Neuropathol. 143, 75–91. https://doi.org/10.1007/s00401-021-02372-6.
Sobue, A., et al., 2021. Microglial gene signature reveals loss of homeostatic microglia associated with neurodegeneration of Alzheimer's disease. Acta Neuropathol. Commun. 9, 1. https://doi.org/10.1186/s40478-020-01099-x.
Srinivasan, K., et al., 2020. Alzheimer's patient microglia exhibit enhanced aging and unique transcriptional activation. Cell Rep. 31, 107843. https://doi.org/10.1016/j.celrep.2020.107843.
Stöberl, N., Maguire, E., Salis, E., Shaw, B., Hall-Roberts, H., 2023. Human iPSC-derived glia models for the study of neuroinflammation. J. Neuroinflammation 20, 231. https://doi.org/10.1186/s12974-023-02919-2.
Stratoulias, V., Venero, J.L., Tremblay, M., Joseph, B., 2019. Microglial subtypes: diversity within the microglial community. EMBO J. 38, e101997. https://doi.org/10.15252/embj.2019101997.
Stupp, R., et al., 2005. Radiotherapy plus Concomitant and Adjuvant Temozolomide for Glioblastoma. N. Engl. J. Med. 352, 987–996. https://doi.org/10.1056/NEJMoa043330.
Subramanian, A., et al., 2017. A next generation connectivity map: l1000 platform and the first 1,000,000 profiles. Cell 171, 1437–1452.e1417. https://doi.org/10.1016/j.cell.2017.10.049.
Suuronen, T., Huuskonen, J., Pihlaja, R., Kyrylenko, S., Salminen, A., 2003. Regulation of microglial inflammatory response by histone deacetylase inhibitors. J. Neurochem. 87, 407–416. https://doi.org/10.1046/j.1471-4159.2003.02004.x.
Tuddenham, J.F., et al., 2024. A cross-disease resource of living human microglia identifies disease-enriched subsets and tool compounds recapitulating microglial states. Nat. Neurosci. https://doi.org/10.1038/s41593-024-01764-7.
Wang, S., Colonna, M., 2019. Microglia in Alzheimer's disease: A target for immunotherapy. J. Leukoc. Biol. 106, 219–227. https://doi.org/10.1002/JLB.MR0818-319R.
Zhao, N., et al., 2022. Elevating microglia TREM2 reduces amyloid seeding and suppresses disease-associated microglia. J. Exp. Med. 219. https://doi.org/10.1084/jem.20212479.